

# PROCEEDINGS OF SPIE

[SPIDigitalLibrary.org/conference-proceedings-of-spie](https://spiedigitallibrary.org/conference-proceedings-of-spie)

## Integrated dielectric scatterers for fast optical classification of biological cells

Alessio Lugnan, Joni Dambre, Peter Bienstman

Alessio Lugnan, Joni Dambre, Peter Bienstman, "Integrated dielectric scatterers for fast optical classification of biological cells," Proc. SPIE 10689, Neuro-inspired Photonic Computing, 1068907 (21 May 2018); doi: 10.1117/12.2306654

**SPIE.**

Event: SPIE Photonics Europe, 2018, Strasbourg, France

# Integrated dielectric scatterers for fast optical classification of biological cells

Alessio Lugnan<sup>\*ab</sup>, Joni Dambre<sup>c</sup>, and Peter Bienstman<sup>ab</sup>

<sup>a</sup>Photonics Research Group, UGent - imec, Technologiepark 15, 9052 Ghent, Belgium

<sup>b</sup>Center for Nano- and Biophotonics (NB-Photonics), Ghent University, Technologiepark 15, 9052 Ghent, Belgium

<sup>c</sup>IDLab, UGent - imec, Technologiepark 15, 9052 Ghent, Belgium

## ABSTRACT

The development of label-free, high-speed, automated and integrated cell sorting solutions is of particular interest for several biomedical applications. The employment of digital holographic microscopy in microfluidic flow cytometry gives access to a large amount of information regarding the 3D refractive index structure of a cell. In the presented work a passive, linear, integrated photonic stage is proposed as an effective nonlinear mixing interface between the hologram projection and the image sensor, allowing for a fast, compact and power-efficient extreme learning machine (ELM) implementation. The required nonlinearity comes from the sinusoid-based transfer function between the phase-shift accumulated by the light through the cell and the field intensity measured by the detector. 2D FDTD simulations with 2 classes of randomized cell models (normal and cancer cells differing in their average nucleus size) have been employed to train and test a readout linear classifier. A collection of silicon nitride pillar scatterers embedded in a silica cladding are interposed between the cell and the intensity monitor, in order to increase the complexity of the acquired interference pattern and to assist the readout linear classifier. The results show that, employing green light, the presence of scatterer layers decreases the classification error rate up to  $\sim 50\%$  with respect to the case without scatterers. Such improvement can be further increased to a factor  $\sim 5$  when a properly designed integrated optical cavity containing the cell is considered. An intuitive argumentation that explains these results is provided.

**Keywords:** Photonic neuromorphic networks, flow cytometry, cell classification, machine learning, extreme learning machine (ELM)

## 1. INTRODUCTION

The employment of digital holographic microscopy in microfluidic flow cytometry is a promising candidate for label-free, high-speed, automated and integrated cell sorting solutions. In this technique, the classification is carried out through the analysis of the interference pattern (hologram) projected by the cell when illuminated by monochromatic light. The hologram is acquired by an image sensor and contains information on the 3D refractive index structure of the cells.<sup>1</sup> The large amount of information contained in a cell hologram enables nontrivial analysis and classifications. On the other hand, the computational cost of elaborating such a complex source of information by reconstructing the image from the hologram is a major hindrance to an increase in the cell sorter throughput, e.g. by parallelization of the process.

An important reduction in the required computing power was achieved by bypassing the reconstruction of the cell image and directly processing the acquired hologram with a machine learning algorithm that carries out the classification task.<sup>1,2</sup> However, a further simplification of the processing in the electric domain is required in order to fully exploit the potential of this implementation.

---

\* alessio.lugnan@ugent.be

## Pillar scatterers for an extreme learning machine (ELM) implementation

We propose a simple collection of integrated dielectric scatterers in a slab waveguide as an interface between the light scattered by a cell and a 1D image sensor, in order to simplify the classification process in the relatively slow electric domain (Fig. 1). In particular, the proposed scatterers are essentially microscopic silica pillars of elliptic cross section embedded in silicon nitride. The whole optical process has been investigated via 2D finite-difference time-domain (FDTD) simulations as a proof-of-concept, approximating the 3D case of a cell flowing in a microfluidic channel interfaced with a photonic chip. The far-field intensity of the light exiting the scatterers cluster is collected by an array of virtual pixels that approximately simulate a line scan image sensor. The pixel outputs are fed into a linear classifier that can be, for example, implemented in the electric domain. The photonic stage containing the scatterers is intended to exploit the nonlinearity of the transfer function that relates the phase shift accumulated by the light through the cell to the corresponding interference pattern measured by an image sensor. Basically, the system can be seen as an hardware implementation of an extreme learning machine (ELM), i.e. a feedforward neural network whose hidden nodes are randomly generated and kept fixed.<sup>3</sup> In the past decade, this machine learning paradigm has been the object of an increasing interest in various research field due to its remarkable efficiency, simplicity, and generalization performance.<sup>4</sup> Generally, the main advantages of ELMs with respect to other machine learning techniques are that only a linear readout (in this case a linear classifier) needs to be trained and that it is easily implemented in hardware. In this case, the pillar scatterer stage determines the ELM hidden node structure by projecting onto the far-field intensity a very intricate nonlinear mapping (based on sinusoidal functions of the phase information). This parallel processing is carried out nearly instantaneously with respect to both the cell movement and the operating speed of an electronic computer, providing an important advantage over other machine learning solutions in the electric domain. It should be stressed that the phase-to-intensity nonlinearity is already expressed by the interference pattern projected by the cell alone, without scatterers. However, the complexity of such a nonlinear mapping can be enhanced and controlled by the use of scatterers in order to increase the performance of a subsequent linear classification. The exploitation of light interference in order to fabricate a passive integrated reservoir computing implementation (which is based on similar principles of ELMs but is applied to time-dependent signals<sup>5</sup>) using linear optical media was demonstrated.<sup>6</sup> However, the time-dependent input information was encoded in the intensity of a laser signal and therefore the transfer function to the output detector was quadratic (amplitude to intensity). Here, the input information is encoded in the phase of a laser signal, such that the readout transfer function can be sinusoidal with respect to that input. The sine, for example, can be profitably employed as activation function in feedforward neural networks under suitable conditions.<sup>7</sup>

## Integrated Fabry-Pérot cavity for enhanced performances

As it will be further discussed in the next section, the classification performance improvement due to the use of scatterers can be enhanced by employing an integrated optical cavity to increase the effective optical path length through the cell, as shown in Fig. 1. Intuitively, this makes the impinging light pass, on average, more than once through the cell. In practice, in the FDTD simulation design 2 Bragg reflectors are placed at the 2 external sides of the microfluidic channel, orthogonally to the light beam direction, creating a Fabry-Pérot cavity. The employed Bragg reflectors are each composed of 3 layers of  $SiO_2$  with a width of  $(455 \pm 10)nm$  in a  $Si_3N_4$  cladding. The error in the layer width was implemented by adding a random value sampled from an uniform probability distribution between 10 and 10 nm. It approximately accounts for fabrication errors. The distance  $D = 21.02\mu m$  between the reflectors was chosen so that the portion of light passing through and near the nucleus of the cell was resonant. This was done by monitoring the light intensity inside the cavity for different values of  $D$ . Note that such a tuning was relatively easy to perform because the cell acts as a weak converging lens, providing an additional light confinement along the microfluidic channel direction.

The reflectivity  $R$  of the reflectors is also a crucial parameter, since it controls the cavity  $Q$ -factor and therefore controls both the sensitivity of the resonance to intracavity optical path lengths and how long the light stays, on average, inside the cavity. This means that by tuning  $R$  a trade-off has to be achieved between how much the phase shift due to the selected resonant cell part is increased and how much the corresponding resonance is stable. In particular, the reflectors employed in the simulations (composed of 3 layers) have a satisfying reflectivity of  $\sim 56\%$ , while it turned out that similar reflectors with 4 and 5 layers have a too high reflectivity, respectively of  $\sim 73\%$  and  $\sim 85\%$ .

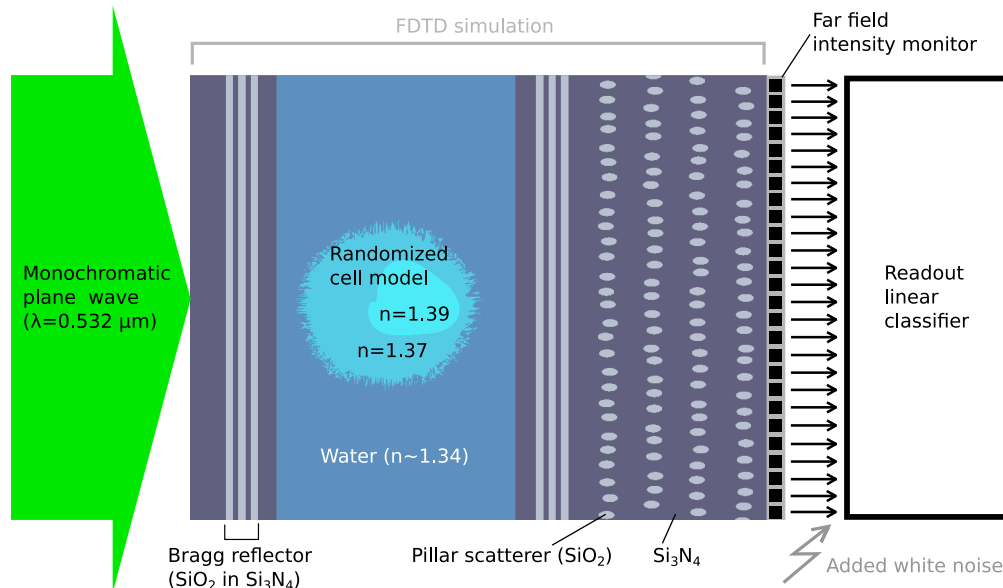


Figure 1. Schematic of the classification process. A monochromatic plane wave impinges on a Fabry-Pérot optical cavity composed by Bragg reflectors and containing a microfluidic channel with a cell in water ( $n_{H_2O} \sim 1.34$ ), which has a low refractive index contrast ( $n_{cytoplasm} = 1.37$ ,  $n_{nucleus} = 1.39$ ); the forward scattered light passes through a collection of silica scatterers ( $n_{SiO_2} \sim 1.461$ ) embedded in silicon nitride ( $n_{Si_3N_4} \sim 2.027$ ) and organized in layers; the radiation intensity is then collected by a far-field monitor, which is divided into bins (pixels); each pixel value is fed into a trained linear classifier (logistic regression) that consists of weighted sums (one per class) of the pixel values. The weights are trained so that the sum exceeds a certain threshold value only if the corresponding input class is recognized.

## Simulation details

A cell in a microfluidic channel, the Fabry-Pérot optical cavity and the proposed silica scatterers were modeled in the same 2D FDTD simulation (Fig. 1) employing Lumerical's FDTD Solutions software. A monochromatic plane wave (vacuum wavelength  $\lambda = 532 \text{ nm}$  as in Ref. 1) of constant intensity impinges transversely on a microfluidic channel ( $15 \mu\text{m}$  wide) filled with water. The channel interfaces with a region containing layers of elliptic scatterers ( $0.5 \mu\text{m}$  wide and  $1 \mu\text{m}$  long) made of  $SiO_2$  embedded in  $Si_3N_4$ . At the end of the scatterer region, a vertical far-field monitor (with an angular resolution of  $55.6 \text{ points/deg}$ ) covers the total length of the simulated space. The simulation region is  $28 \mu\text{m}$  long along the vertical direction and from  $20 \mu\text{m}$  to  $30 \mu\text{m}$  along the horizontal direction, depending on the number of scatterer layers. The FDTD mesh size is  $\sim \lambda/29$ . 2D randomized cell models were employed to approximately simulate the refractive index of cytoplasm and nucleus. The scatterers are placed in vertical layers with an average vertical distance of  $1 \mu\text{m}$  between their centers. The center of each scatterer is randomly displaced with respect to their unperturbed center in the layer, both along the vertical and the horizontal directions. All the random displacements belonging to the same architecture were sampled from the same uniform probability distribution. The random displacement amplitude were used to tune the complexity of the scattering mixing action, optimizing the corresponding ELM effectiveness. More details about the employed cell models and the scatterer configuration are described in Ref. 8, with the exception that the simulation time had to be properly increased to  $1.2 \text{ ps}$  when the optical cavity was included in the design. It should be stressed that the scope of this work is to provide a proof-of-concept of a new approach to photonics machine learning, that can be generalized to many other implementations besides the discussed examples. Therefore, the dimensionality of the simulation, the size of the structures and the cell model are a consequence of a trade-off between closeness to reality, saving of computational time and the search of a sufficiently complex (but not overly so) task. In any case, all the simulated objects, aside from the scatterers, were designed independently of the classification results.

## Machine learning details

The far-field intensity profile was divided into  $N_{pix}$  bins (or pixels) and the integration over each bin was fed into a logistic regression. The Scikit-learn Python library<sup>9</sup> was employed, using the “liblinear” solver. For each tested scatterer configuration a number  $N_{samp}$  of simulations was performed randomly varying the cell shape, as described in the previous section. In particular, the classification results reported in the next section are obtained from sample sets of  $N_{samp} = 3200$  samples each. In half of the  $N_{samp}$  simulations a “normal” cell was considered (average nucleus radius of  $1.2\mu m$ ), while in the remaining half a “cancer” cell (with bigger average nucleus radius of  $2.5\mu m$ ) was used. 75% of these two sets was employed in the training of the logistic regression, while the rest was used as test set. The names in quotation marks were chosen because of the common tendency of cancer cells to show evident irregularities in nucleus size.<sup>10</sup>

Gaussian white noise was added a posteriori on the interference patterns before they were divided into bins. Different values for the noise standard deviation were chosen: 1%, 5%, 10%, 20%, 30%, 50% and 100% of the average intensity over the sample set.

A study on the dependence of the classification test error on the regularization strength (L1 and L2) and on  $N_{samp}$  was carried out in the two cases with and without the use of scatterers, on a set of 2000 samples each. For this investigation, a 4 layer scatterer configuration was considered, with  $A_r = 150nm$  and  $D = 1.846\mu m$  (this particular configuration was one of the best performing in a preliminary exploration based on a lower (800) number of samples). The study pointed out that regularization had no significant positive effect on the performances of the two classification tasks. Furthermore, it showed that the learning curve (test error v.s. number of samples) converged around  $N_{samp} = 800$  when the scatterers were used. Thus, for the classifications presented in the next section no regularization was considered, but the investigation on the effect of different noise levels partially covers the topic at least with regard to the L2 regularization. The classification dependence on the number of pixels and training epochs was instead kept under direct control by performing sweeps for each tested configuration.

The presented results are obtained through a validation process in which the simulated data samples are randomly shuffled before they are split into training and test sets. From the results generated by repeating this procedure 20 times a mean value and a confidence interval (chosen as  $\pm$  twice the standard deviation) were calculated and plotted. Note that a different noise vector is added to the intensity profiles after each shuffling.

## 2. RESULTS AND DISCUSSION

### Classification without optical cavity

Let us consider a green laser source ( $\lambda = 532nm$ ) without introducing the optical cavity in the simulation design. Let us compare the classification error on the test samples when no scatterers are present and when, instead, 4 scatterer layers are employed (further classification details are as in Ref. 8). The resulting error rate values for different numbers of pixels and for different noise levels (Fig. 2 a) show that the use of scatterer layers allows for a significant error rate reduction (up to  $\sim 50\%$ ), provided that a sufficient number of pixels and a low enough noise level are considered.

Even if significant improvements due to the introduction of pillar scatterers are achieved, a simple quantitative reasoning on how nucleus size changes affect the input of the readout classifier suggests that better results can be in principle obtained. In particular, the difference in phase shift accumulated by the light through the 2 types of nucleus corresponding to the 2 cell classes is too small and therefore is expressed in an almost linear way by the acquired intensity pattern, while nonlinearity is required by the ELM approach (see Ref. 8 under *Nonlinear phase sensitivity* in *Results and discussion* section). The employment of an UV laser source ( $\lambda = 337.1nm$ ), that implies an increase in the optical path through the given nuclei, can be considered as a solution and much better classification performance are obtained (Fig. 2 b). However, when real applications are concerned, this option is highly impractical as UV lasers are usually quite expensive and would probably damage or even kill the illuminated cells.

### Classification with optical cavity

A more feasible solution consists of increasing the effective optical path length through the cell by inserting it in the Fabry-Pérot optical cavity presented in the previous section. In this case, the sensitivity of the acquired

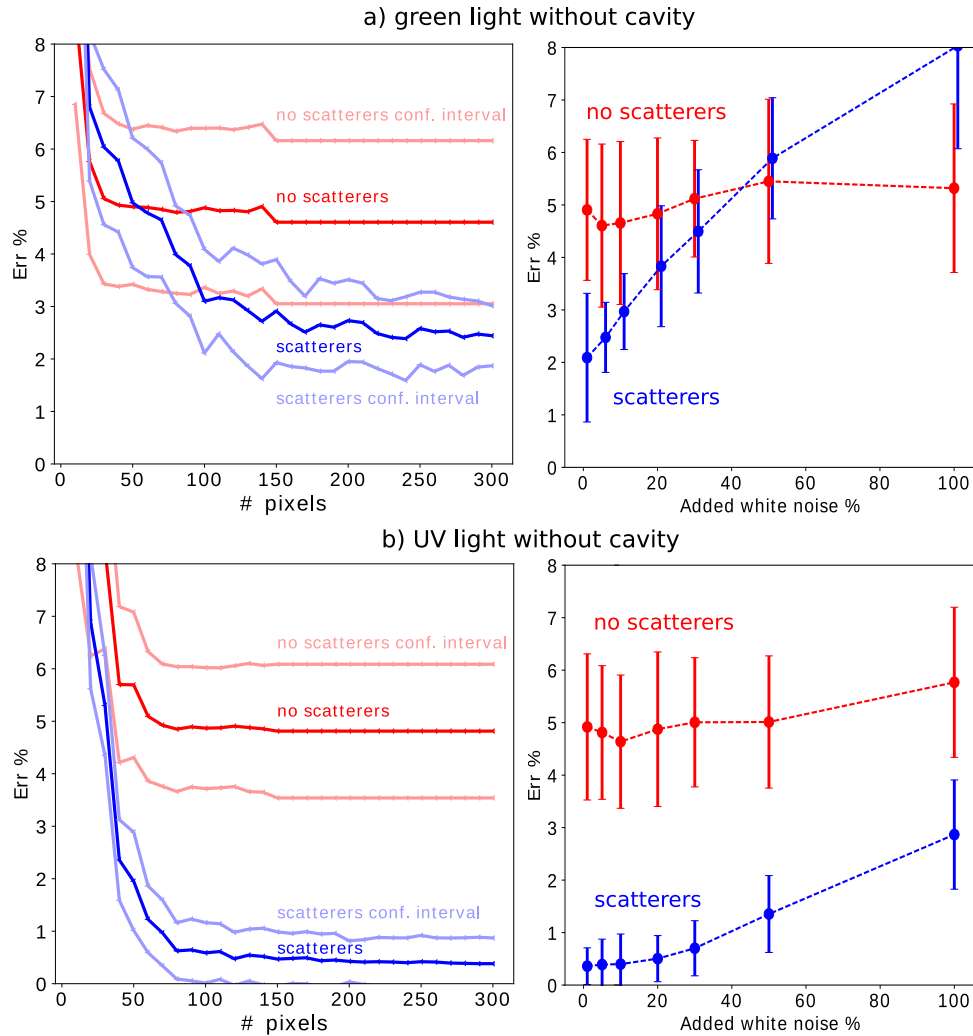


Figure 2. Comparison between the test error rates of “normal” and “cancer” cell classification, corresponding to the absence (in red) and the presence (in blue) of scatterers. **a)** A green laser source ( $\lambda = 532nm$ ) is employed. **b)** An UV laser source ( $\lambda = 337.1nm$ ) is employed. On the left: test error rate as a function of the number of employed pixels, with 5% added white noise. The darker and the lighter versions of the two line colors respectively represent the mean value and the confidence interval (of 2 standard deviations) over the 20 sample sets generated for validation. On the right: test error rate (averaged on the values obtained considering  $N_{pix} = 250, 260, \dots, 300$ ) as a function of the added noise percentage.

intensity pattern to the nucleus size can be improved by increasing the average time that the resonant light passing through the nucleus stays in the cavity. On the other hand, if the cavity  $Q$ -factor is too high, the resonance strength might be strongly influenced by uninteresting small details of the cell structure or by fabrication errors. Generally, the cavity should be designed so that the average light phase shift differences due to the optical feature of interest corresponding to the considered classes are roughly between  $\pi/2$  and  $2\pi$ . Indeed, a phase shift difference significantly lower than  $\pi/2$  would induce a nearly linear difference on the acquired intensity pattern, undermining the nonlinearity requirement of the ELM approach. On the other hand, a phase shift difference significantly bigger than  $2\pi$  would make the acquired intensity pattern too sensitive to uninteresting small changes in the cell optical features, undermining the stability requirement of the ELM approach.

Fig. 3 shows the simulation results obtained from the use of green light in combination with the presented Fabry-Pérot cavity. A substantial improvement is observed with respect to the green source case without cavity (Fig. 2 a). In particular, the classification improvement due to the use of scatterers is increased by a factor 5

by the cavity, for sufficiently low but still plausible noise levels ( $< 10\%$ ). At these noise levels, the results are similar to what was obtained with an UV light source (Fig. 2 b), without the drawback of possible cell damage. For higher noise levels an increased sensitivity to noise pushes the classification error rate to significantly higher values.

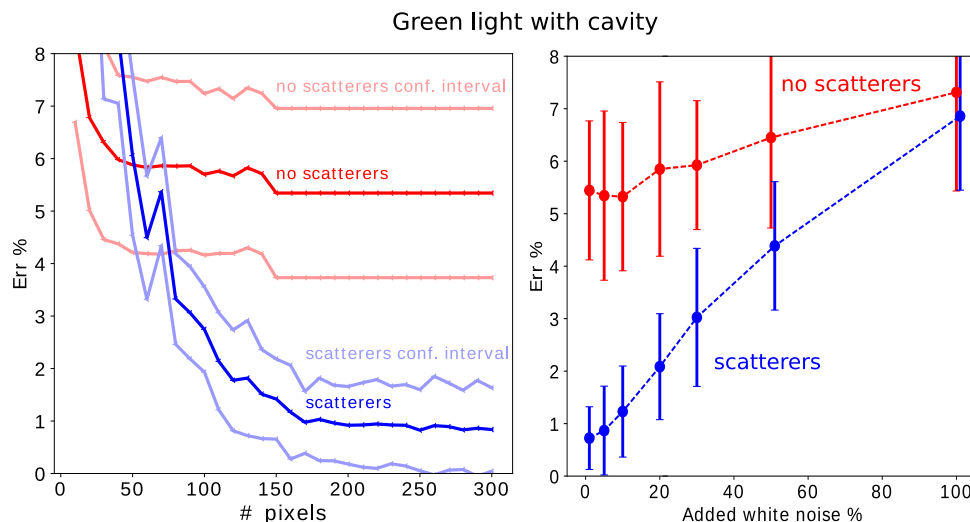


Figure 3. Comparison between the test error rates of “normal” and “cancer” cell classification, corresponding to the absence (in red) and the presence (in blue) of scatterers. A green laser source ( $\lambda = 532nm$ ) is employed and the integrated optical cavity is now included in the simulation design. On the left: test error rate as a function of the number of employed pixels, with 5% added white noise. The darker and the lighter versions of the two line colors respectively represent the mean value and the confidence interval (of 2 standard deviations) over the 20 sample sets generated for validation. On the right: test error rate (averaged on the values obtained considering  $N_{pix} = 250, 260, \dots, 300$ ) as a function of the added noise percentage.

### 3. CONCLUSIONS

In this work, a simple passive integrated photonic structure is proposed to improve the performance of a linear classifier employed for the optical classification of different cell kinds. The presented approach enables for significant reduction of the computational cost required for both training and application of the classifier, with respect to an equivalent application in the electric domain.

The proposed integrated structure consists of a collection of silica pillars embedded in silicon nitride that scatters the monochromatic light diffracted by a cell. When a green laser source is employed, the scatterers presence leads to a significant improvement in performance (up to 50%) of the classification of simulated cells with different nucleus size, provided that a sufficient number of pixels and a low enough noise level are considered. When an UV laser source ( $\lambda = 337.1nm$ ) is employed, the scatterers presence leads to a much greater error rate reduction (up to an order of magnitude) for all the considered pixel numbers and noise levels.

The much more feasible implementation with green light, though, is improved to a performance (a factor  $\sim 5$  improvement) similar to the one obtained with UV light, if an integrated Fabry-Pérot optical cavity is properly designed and included in the simulation. The main advantage arising from the use of the optical cavity is that it can be designed to increase the acquired intensity pattern sensitivity towards specific details in the refractive index structure of a cell. This can make the optical features of interest more evident to the readout classifier with respect to other competing ones.

## REFERENCES

- [1] Lagae, L., Verduyck, D., Dusa, A., Liu, C., de Wijs, K., Stahl, R., Vanmeerbeeck, G., Majeed, B., Li, Y., and Peumans, P., “High throughput cell sorter based on lensfree imaging of cells,” in [*2015 IEEE International Electron Devices Meeting (IEDM)*], 13.3.1–13.3.4 (Dec 2015).
- [2] Schneider, B., Vanmeerbeeck, G., Stahl, R., Lagae, L., Dambre, J., and Bienstman, P., “Neural network for blood cell classification in a holographic microscopy system,” in [*2015 17th International Conference on Transparent Optical Networks (ICTON)*], 1–4 (July 2015).
- [3] Huang, G.-B., Zhu, Q.-Y., and Siew, C.-K., “Extreme learning machine: Theory and applications,” *Neurocomputing* **70**(1), 489 – 501 (2006). Neural Networks.
- [4] Huang, G., Huang, G.-B., Song, S., and You, K., “Trends in extreme learning machines: A review,” *Neural Networks* **61**, 32 – 48 (2015).
- [5] Lukoeviius, M. and Jaeger, H., “Reservoir computing approaches to recurrent neural network training,” *Computer Science Review* **3**(3), 127 – 149 (2009).
- [6] Vandoorne, K., Mechet, P., Vaerenbergh, T. V., Fiers, M., Morthier, G., Verstraeten, D., Schrauwen, B., Dambre, J., , and Bienstman, P., “Experimental demonstration of reservoir computing on a silicon photonics chip,” *Nat. Commun.* **5**(3541) (2014).
- [7] Wong, K. W., Leung, C. S., and Chang, S. J., “Use of periodic and monotonic activation functions in multilayer feedforward neural networks trained by extended kalman filter algorithm,” *IEE Proceedings - Vision, Image and Signal Processing* **149**, 217–224 (Aug 2002).
- [8] Lugnan, A., Dambre, J., and Bienstman, P., “Integrated pillar scatterers for speeding up classification of cell holograms,” *Opt. Express* **25**, 30526–30538 (Nov 2017).
- [9] Pedregosa, F., Varoquaux, G., Gramfort, A., Michel, V., Thirion, B., Grisel, O., Blondel, M., Prettenhofer, P., Weiss, R., Dubourg, V., Vanderplas, J., Passos, A., Cournapeau, D., Brucher, M., Perrot, M., and Duchesnay, E., “Scikit-learn: Machine learning in python,” *J. Mach. Learn. Res.* **12**, 2825–2830 (Nov. 2011).
- [10] Zink, D., Fischer, A. H., and Nickerson, J. A., “Nuclear structure in cancer cells,” *Nature reviews cancer* **4**(9), 677 (2004).